EARTH SURFACE PROCESSES AND LANDFORMS
Earth Surf. Process. Landforms **40**, 389–402 (2015)

Published online 18 September 2014 in Wiley Online Library
(wileyonlinelibrary.com) DOI: 10.1002/esp.3640

Very slow erosion rates and landscape preservation across the southwestern slope of the Ladakh Range, India

Craig Dietsch,[1]* Jason M. Dortch,[2] Scott A. Reynhout,[1] Lewis A. Owen[1] and Marc W. Caffee[3]
[1] Department of Geology, University of Cincinnati, Cincinnati, OH 45221, USA
[2] School of Environment, Education, and Development, The University of Manchester, M0 1QD, UK
[3] Department of Physics/PRIME Laboratory, Purdue University, West Lafayette, IN 47906, USA

Received 25 October 2012; Revised 8 July 2014; Accepted 30 July 2014

*Correspondence to: C. Dietsch, Department of Geology, University of Cincinnati, Cincinnati, OH 45221, USA. E-mail: dietscc@ucmail.uc.edu

ESPL
Earth Surface Processes and Landforms

ABSTRACT: Erosion rates are key to quantifying the timescales over which different topographic and geomorphic domains develop in mountain landscapes. Geomorphic and terrestrial cosmogenic nuclide (TCN) methods were used to determine erosion rates of the arid, tectonically quiescent Ladakh Range, northern India. Five different geomorphic domains are identified and erosion rates are determined for three of the domains using TCN ^{10}Be concentrations. Along the range divide between 5600 and 5700 m above sea level (asl), bedrock tors in the periglacial domain are eroding at 5.0 ± 0.5 to 13.1 ± 1.2 meters per million years (m/m.y.)., principally by frost shattering. At lower elevation in the unglaciated domain, erosion rates for tributary catchments vary between 0.8 ± 0.1 and 2.0 ± 0.3 m/m.y. Bedrock along interfluvial ridge crests between 3900 and 5100 m asl that separate these tributary catchments yield erosion rates $<0.7 \pm 0.1$ m/m.y. and the dominant form of bedrock erosion is chemical weathering and grusification. Erosion rates are fastest where glaciers conditioned hillslopes above 5100 m asl by over-steepening slopes and glacial debris is being evacuated by the fluvial network. For range divide tors, the long-term duration of the erosion rate is considered to be 40–120 ky. By evaluating measured ^{10}Be concentrations in tors along a model ^{10}Be production curve, an average of ~24 cm is lost instantaneously every ~40 ky. Small (<4 km^2) unglaciated tributary catchments and their interfluve bedrock have received very little precipitation since ~300 ka and the long-term duration of their erosion rates is 300–750 ky and >850 ky, respectively. These results highlight the persistence of very slow erosion in different geomorphic domains across the southwestern slope of the Ladakh Range, which on the scale of the orogen records spatial changes in the locus of deformation and the development of an orogenic rain shadow north of the Greater Himalaya. Copyright © 2014 John Wiley & Sons, Ltd.

KEYWORDS: Ladakh Range; erosion rates; Be-10; geomorphic zones; old landscapes

Introduction

The spatial variability of erosion and the timescales over which different processes of erosion operate play fundamental roles in the evolution of mountain landscapes and topography. Topography evolves through the extent and efficacy of erosive fluvial, glacial, and hillslope processes that are driven and modified by climatic and tectonic feedbacks. A seminal example of the dynamism between erosional processes and topography is the correlation between the mean Quaternary equilibrium-line altitude (ELA) of valley glaciers and zones of focused erosion, summit elevations, and peak hypsometric surface area (Montgomery *et al.*, 2001; Mitchell and Montgomery, 2006; Berger and Spotila, 2008; Egholm *et al.*, 2009; Spotila, 2013). These correlations suggest that glacial erosion limits the vertical development of mountain topography to an elevation within several hundred meters of the mean Quaternary ELA (Brozović *et al.*, 1997; Spotila, 2013 and references therein), although there are notable exceptions (Thomson *et al.*, 2010). Glaciers can condition landscapes for their subsequent erosive evolution by modifying topography and changing the area available for snow and ice accumulation, thus decreasing subsequent glacial extent given similar climatic forcing or disproportionally increasing glacier extent with stronger climatic forcing (Kaplan *et al.*, 2009; Pedersen and Egholm, 2013). Because glaciers can control the distribution of sediment, they can dictate postglacial fluvial dynamics (Norton *et al.*, 2010; Hobley *et al.*, 2010) that drive streams to modify their channels, often towards re-establishing an equilibrium gradient (Korup and Montgomery, 2008).

The lower elevation limit of glaciation in mountains broadly defines a boundary above which the processes and rates of erosion, principally glacial and periglacial, differ significantly from those at lower altitudes controlled dominantly by streams. On the scale of individual catchments across a single mountain slope, non-uniform erosion can occur among catchments shaped by streams or glaciers (Stock *et al.*, 2006). In the very upper reaches of glaciated valleys adjacent to ridgelines and mountain summits, glacial headwall erosion as well as slope processes in cirques can modify divides (Oskin and Burbank, 2005; Dortch *et al.*, 2011a; Spotila, 2012) and affect peak elevation (Anderson, 2005; Ward *et al.*, 2012). Post-glacial trunk streams can erode or aggrade which can set boundary conditions for hillslope erosion (Burbank *et al.*, 1996; Whipple, 2004) and can modify tributary catchments. In this way, topographic and morphologic domains develop and relief evolves across a mountain system, controlled by different geomorphic processes over Quaternary or longer timescales. In the short term ($10^{3\text{-}5}$ y), non-uniform erosion can reflect variations in a variety of factors, including climate (Huntington *et al.*, 2006), faulting (Riebe *et al.*, 2001), and stream power (Finnegan *et al.*, 2008). Over longer timescales, orogens can evolve towards a topographic steady-state (Pazzaglia and Brandon, 2001; Willet and Brandon, 2002) in which systematic topographic changes driven by erosion balance tectonically-driven mass influx.

The Himalayan-Tibetan orogen is one of the world's premier laboratories to investigate spatial and temporal patterns of erosion and their underlying causality (Lavé and Avouac, 2001; Vannay *et al.*, 2004; Thiede *et al.*, 2005) because of its high elevation and relief, active tectonics, and pronounced precipitation gradient. In addition, there is an extensive chronology of glaciation in many parts of the orogen (summarized by Dortch *et al.*, 2013 and Murari *et al.*, 2014). In the high-precipitation monsoon-influenced Greater Himalaya, erosive landscape features are dominated by the effects of Late Quaternary and Holocene glaciation and high rates of post-glacial fluvial incision (Leland, *et al.*, 1998; Shroder and Bishop, 2000; Vannay *et al.*, 2004; Adams *et al.*, 2009). Glacial and non-glacial landforms and sediments with ages greater than several tens of thousands of years in this part of the orogen are uncommon (Owen *et al.*, 2005, 2008; Owen and Dortch, 2014), likely due to reworking and erosion by fluvial and hillslope processes. Throughout the Indian Himalayan, Holocene rates of fluvial incision typically exceed 5000 m/m.y., reflecting changes in monsoon intensity and deglaciation events, and the Himalayan Holocene average is 9000 ± 4.9 m/m.y. Longer-term Late Quaternary incision rates are ≤ 5000 m/m.y. (Dortch *et al.*, 2011b).

In arid parts of the Himalayan-Tibetan orogen, bedrock erosion rates can be extremely slow; for example, <100 m/m.y. in the Tibetan Plateau (Lal *et al.*, 2003). Slow erosion rates might also be expected in the arid Ladakh Range of the Transhimalaya in northern India, which has been tectonically quiescent since the Miocene (Kirstein *et al.*, 2006, 2009). The main trunk valleys of the Ladakh Range have been glaciated and some moraines reach all the way into the Indus Valley. In the Indus Valley and elsewhere in Ladakh, glacial landforms with ages of hundreds of thousands of years are preserved (Owen *et al.*, 2006; Hedrick *et al.*, 2011). Nevertheless, incised valleys in the Ladakh Range can have >1 km of relief and peaks can exceed 6000 m above sea level (asl). Despite being in the rain shadow of the Greater Himalaya, precipitation across Ladakh can be strongly affected by the monsoon (Bookhagen *et al.*, 2005; Hobley *et al.*, 2012) and the Ladakh Range has been subjected to enhanced monsoons throughout the Quaternary (Gasse *et al.*, 1996; Shi *et al.*, 2001).

The Ladakh Range, then, provides a distinctive setting in the Himalayan-Tibetan orogen to examine the spatial variation in processes and rates of erosion across geomorphic domains. In addition, despite much regional work little is known about how large-scale tectonic movements influence surficial erosional processes and the development and preservation of small-scale landscapes. By estimating the time-averaged duration of erosion rates, it is possible to evaluate whether the erosive history of the Ladakh Range can be temporally linked to post-Miocene crustal thickening of the high ranges to the south of Ladakh (Catlos *et al.*, 2001; Wobus *et al.*, 2005) and the development of the orogen's characteristic rain shadow (Bookhagen and Burbank, 2006; Anders *et al.*, 2006).

We apply geomorphic, remote sensing, and TCN ^{10}Be methods to evaluate landscape and topographic development in contrasting glaciated and unglaciated domains across the southwestern slope of the Ladakh Range. Hobley *et al.* (2010) defined three domains reflecting the dominant mode of channel behavior. We base our sampling on four geomorphic domains defined principally on the morphology of hillslopes and stream channels. The geomorphology of each of our domains is dominated by a different glacial, periglacial, or fluvial process. Using the *Area x Altitude* method of Osmaston (1994), we reconstruct the most extensive glacial stage, the Leh glacial stage, to further define glaciated and unglaciated domains in this part of the Ladakh Range (Figure 1). In addition, we characterize various landscape features and the dominant geomorphic processes from the main range divide downslope to the Indus Valley to assess erosive processes, and evaluate their relationship to topography and relief. In doing so, we rename Hobley *et al.*'s (2010) three geomorphic domains and add a fourth. Our data allow us to quantify local relief production and the timescales of landscape evolution in different geomorphic domains, and to qualitatively describe the sediment budget downslope from the glaciated to the unglaciated domains. Our work adds to a small number of studies that quantify changes in relief in the Himalayan-Tibetan orogen (Montgomery, 1994; Strobl *et al.*, 2012). Bedrock erosion rates are highest at high elevation astride the divide of the Ladakh Range and lowest along unglaciated slopes at lower elevation where the present relief has persisted throughout the Quaternary and likely for much longer.

Regional Setting

The Ladakh Range trends NW-SE, with a width of ≤ 50 km, bounded to the southwest by the Indus Suture Zone (ISZ) and to the northeast by the Karakoram fault and the Shyok Suture Zone (Steck, 2003); only the Karakoram fault is still active (Brown *et al.*, 2002; Chevalier *et al.*, 2005). The Ladakh Range is underlain by essentially homogeneous bedrock composed of Cretaceous continental-arc granodiorite of the Ladakh batholith (Searle, 1991). Relief ranges from 3000 to >6000 m above asl. The Ladakh Range has a pronounced morphometric asymmetry with greater basin size, valley width, and mean elevation north of the range divide (Dortch *et al.*, 2011a). Jamieson *et al.* (2004) and Kirstein (2011) attributed this asymmetry to the northward propagation of the ISZ, which induced the range to tilt southwards along its long axis. Apatite and zircon (U-Th)/He and fission track thermochronometric data from samples collected across the area shown in Figure 1 reveal that rock cooling of the southwestern slope of the Ladakh Range took place during the Oligocene and Early Miocene (Kirstein *et al.*, 2006, 2009). From age–elevation profiles and thermal modeling, Kirstein *et al.* (2009) calculated Oligocene through Pliocene exhumation rates of between 400 and 750 m/m.y. For the same area, Kumar *et al.* (2007) used age–elevation apatite and zircon fission track age data to calculate an exhumation rate of 100 m/m.y. between 25 and 9 Ma, assuming a constant 30 °C/km geotherm, and with some scatter of lower elevation data points. Kirstein *et al.*'s (2009) modeling results show that from the Middle Miocene, the cooling rate of exhuming rocks slows to <4 °C/m.y.

On the southwestern-facing side of the range geomorphic features indicate that there has been little uplift here during much of the Quaternary: alluvial fans, small peaks on buried

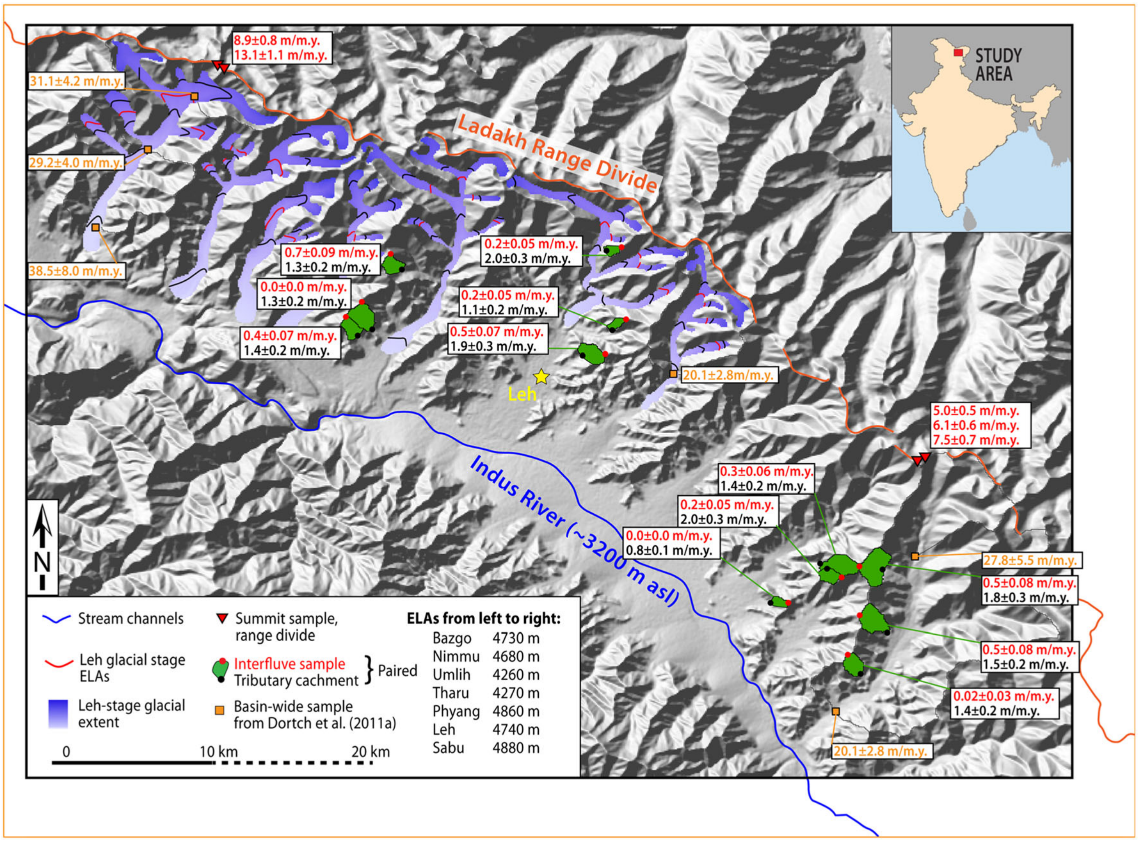

Figure 1. 90 m SRTM DEM of the southwestern slope of the Ladakh Range showing sampling locations, ^{10}Be-based erosion rates, and reconstruction of the Leh glacial stage. Colored shapes show the location of various samples. Red triangles along the Ladakh Range divide are bedrock tor samples. Green areas are tributary catchments that drain into trunk streams that reach the Indus River. The red and black circles touching these tributary catchments are interfluvial bedrock samples collected along ridge crests and catchment sediment samples, respectively. Orange squares are sediment samples from trunk streams yielding catchment-wide erosion rates determined by Dortch *et al.* (2011a). Valleys shaded in purple show reconstructed glaciers during the Leh glacial stage; see text for discussion. The maximum down valley extent of Leh glacial stage glaciers at ~ 310 ka is from Owen *et al.* (2006). Red contours show the location of Leh glacial stage area-altitude ELAs. Black contours follow 500 m intervals with the uppermost black contour equal to 5000 m asl. The Leh glacial stage reconstruction shows that the tributary catchments we sampled were not glaciated. Kirstein *et al.*'s (2006, 2009) apatite and zircon (U-Th)/He and fission track samples were collected across the area, from the Bazgo valley in the northwest to the unnamed valley in the southeast below our three southeastern most tributary catchments. This figure is available in colour online at wileyonlinelibrary.com/journal/espl

spurs, and aggrading streams at lower elevation, and highly denuded mountain ridges and spurs at higher elevation (Dortch *et al.*, 2011a). Based on surface exposure ages >60 ka of strath terraces along the Indus River bordering our field area, the mean rate of fluvial incision of the Indus has been <400 ± 0.04 m/m.y. (Dortch *et al.*, 2011b) and there has been extensive sediment accumulation in the Indus Valley astride the central Ladakh Range (encompassing our study area). Alluvial fans from the Zanskar Range prograde northwards across the valley and sediment aggrades in trunk streams in the lower reaches of the Ladakh Range (Hobley *et al.*, 2010), both processes promoting lateral translation of the Indus Valley and Indus River towards the southwestern flank of the Ladakh Range (Jamieson *et al.*, 2004).

Since at least the mid-Miocene, then, denudation of the Ladakh Range south of the range divide has been very slow, attributed to tectonic quiescence in concert with down-to-the-southwest tilting (Dortch *et al.*, 2011a; Kirstein, 2011), blanketing of catchments by sediment, and long-term aggradation (Jamieson *et al.*, 2004). The tectonic quiescence of the Ladakh Range since the Early Miocene is in sharp contrast to the record of Plio-Pleistocene active faulting and exhumation in the high-precipitation monsoon-influenced Greater and Lesser Himalaya to the south of Ladakh in India, such as in Lahul and Garhwal (Sorkhabi *et al.*, 1999; Vannay *et al.*, 2004; Adams *et al.*, 2009). Uplift of the Greater Himalayan in Lahul and Garhwal has been described by models of mid-crustal channel flow (reviewed by Godin *et al.*, 2006 and Harris, 2007) that took place principally during the Early to Middle Miocene and by simple thrusting over a mid-crustal ramp (Godard *et al.*, 2006) as young as Pliocene (Catlos *et al.*, 2001).

Summer precipitation in the Ladakh Range is largely controlled by northward propagation of the Indian summer monsoon whereas winter precipitation is driven by the mid-latitude westerlies (Benn and Owen, 1998; Owen, 2009). The mean precipitation at the city of Leh (34°09′N, 77°34′E, 3514 m asl) is ~115 mm/y where the average maximum diurnal temperature range is −2.8 °C to −14 °C in January and 24.7 °C to 10.2 °C in July (Osmaston, 1994). Weather records from the airport at Leh have yielded average summer (June to September) and winter (December to March) precipitation of about 40 and 30 mm, respectively, over the past six decades (Weatherbase.com, 2013). Climatic data are not available for elevations higher than Leh, but TRMM data (Bookhagen and Burbank, 2006) indicate that mean rainfall throughout the range is < 500 mm/y. Based on lake core data and other proxy records (Gasse *et al.*, 1996; Shi *et al.*, 2001), northern India including the Ladakh Range has been affected by enhanced monsoons throughout the Quaternary. In addition, along the southwestern flank of the range, in the vicinity of Leh, a short-lived, intense rainstorm in August 2010 produced debris flows and landslides; Hobley *et al.* (2012) calculated that at least 75 mm of rain fell in 30 min.

Glacial history of the Ladakh Range

The preserved glacial record in the Ladakh Range is one of progressively smaller glacial advances after ~430 ka (Owen *et al.*, 2006). Based on TCN ^{10}Be ages of moraine boulders, Owen *et al.* (2006) concluded that the Leh glacial stage moraines of Fort (1983) south of the divide formed before or during MIS-6 but more recently, Dortch *et al.* (2013) recalculated the age of the Leh stage moraines to be 311 ± 32 ka. These Leh stage glacial moraines indicate a Late Quaternary ELA depression of less than ~1000 m; Burbank and Fort (1985) and Dortch *et al.* (2011a) estimated the modern ELA at 5280 and 5455 ± 130 m asl, respectively, south of the range divide.

To further define former glacier extent and to delimit glaciated and unglaciated domains in this part of the Ladakh Range, we reconstructed the Leh stage glacial system (Figure 1). The Leh glacial stage was chosen because it is the most extensive glacial stage in the region with well preserved terminal moraines in seven valleys (Owen *et al.*, 2006), which are critical for balancing glacial tributary systems with reconstructed ELAs. Leh glacial stage deposits have not been identified in the field or on remote sensed imagery east of the Sabu Valley (Figure 1) so we cannot accurately test the validity of our glacial reconstruction for the easternmost region of our field area.

Based on the fact that Leh stage glaciers had multiple tributaries and the lack of evidence suggesting that they were mantled by debris (Leh stage moraines are not hummocky, which commonly form from debris mantled ice or incorporation of previous moraines), we used the median elevation or AA method as outlined and recommended by Osmaston (2005) to reconstruct Leh glacial stage ELAs. We employed an iterative process whereby the glacial system is overestimated by assuming every tributary contained an accumulation zone. The glacier hypsometry is then calculated using 90 m Shuttle Radar Topography Mission (SRTM) digital elevation models (DEMs), and the ELA is then calculated and plotted onto the estimated glacier outline. Tributary valleys below the ELA would not have an accumulation zone and are removed from the modeled glacial system (Dortch *et al.*, 2009, 2010). This process is repeated until a portion of all tributary valleys is above the reconstructed glacier ELA.

Geomorphic Domains, Field Observations, and Sampling Strategy

Domain 1 of Hobley *et al.* (2010) includes the upper reaches of glaciated catchments that are U-shaped valleys draped by paraglacial fans with hummocky floors; we rename this domain the 'periglacial domain' (following the terminology of Slaymaker, 2011). At elevations below the periglacial domain, a set of linear valleys are occupied by trunk streams whose power is high enough to transport glacial sediment and incise gorges into their valley floors: this is domain 2 of Hobley *et al.* (2010) which we rename the 'paraglacial domain'. Erosion rates for trunk streams in the paraglacial domain range between 20 and 40 m/m.y. (Dortch *et al.*, 2011a). Below the paraglacial domain, fluvial aggradation characterizes the trunk stream valleys as they approach and drain into the Indus River; this is domain 3 of Hobley *et al.* (2010), which we rename the 'aggradation domain'. The trunk streams have side tributaries that drain small catchments that we recognize as a fourth domain. Based on our reconstruction of Leh stage glaciation and field observations (described in detail below), these tributary catchments have not been glaciated within the last glacial cycle and so we name these small catchments and their interfluvial ridges the 'unglaciated domain'. Figure 2 shows a generalized plan view of the geomorphic domains and their major features. We collected samples for TNC ^{10}Be analysis from the periglacial and unglaciated domains, which are described in further detail below. It should be noted that our domains reflect the current geomorphology of the landscape and will change spatially through time due to climatic and tectonic perturbations.

Periglacial domain; sampling range divide tors

In the Ladakh Range, granodiorite tors on the range divide form local bedrock 'landscapes' where denudation is weathering-limited (Small *et al.*, 1997; Kober *et al.*, 2007). Following the formation and exposure of the tors, physical and chemical weathering, and mass movements can lower these bedrock summits. Range divide ridges and the tors along them have evolved from drainage divides as hillslopes were over-steepened through glacial headwall erosion and mass wasting (Anderson, 2002; Oskin and Burbank, 2005; Spotila, 2012). These erosive processes are active, dominantly in cirques on the north side of the range divide where north-side glaciers erode through the divide, capturing catchments (Dortch *et al.*, 2011a) and creating new fields of range divide bedrock ridges along which tors develop. The range divide tors we observed can be strongly fractured, surrounded by toppled blocks and skirts of pebble-sized and smaller angular debris that are smaller than the bedrock joint and fracture spacing (Figure 3(A)). Some very large tor tops have 10–20 cm thick exfoliated sheets developed across their surfaces. The vast majority of sediment along the range divide occurs on angular talus slopes including the skirts of pebble-sized angular debris. The tors and talus slopes along the range divide suggest that the predominant modes of physical weathering along these summits are block removal and bedrock shattering. At ~5400 m asl where slope angles decrease, large talus fields descend into valley bottoms and begin to give way to permafrost, soil, small-scale patterned ground, and frost-heaved blocks indicating that freeze-thaw processes are active. Talus cones cut across streams and are not fluvially incised; instead, fine-grained sediments are filtered out and accumulate on the upstream edge of the talus cones. We demarcate this difference in erosional processes by subdividing the periglacial domain into two parts: high ridges where shattering and block removal is dominant (periglacial domain A; Figure 2), and high valley bottoms where talus aggrades and slope and freeze-thaw processes are dominant (periglacial domain B, Figure 2). Using ^{10}Be concentrations, we determined bedrock erosion rates along the divide of the Ladakh Range by sampling the tops of five tors (Figure 1; Table I). Samples were collected only from tors standing >1 m along the divide to minimize the likelihood of past burial and snow cover.

Unglaciated domain: sampling interfluve bedrock ridges and tributary catchment sediments

Hillslopes of tributary catchments above the trunk streams that drain the southwestern slope of the Ladakh Range are characterized by weathering of exposed bedrock (Figure 3(B), C)) but only local sediment transport along hillslopes. Tributary catchments descend from narrow interfluve bedrock ridges that lack tors. Compared with the range divide, the interfluve bedrock ridges we sampled record important

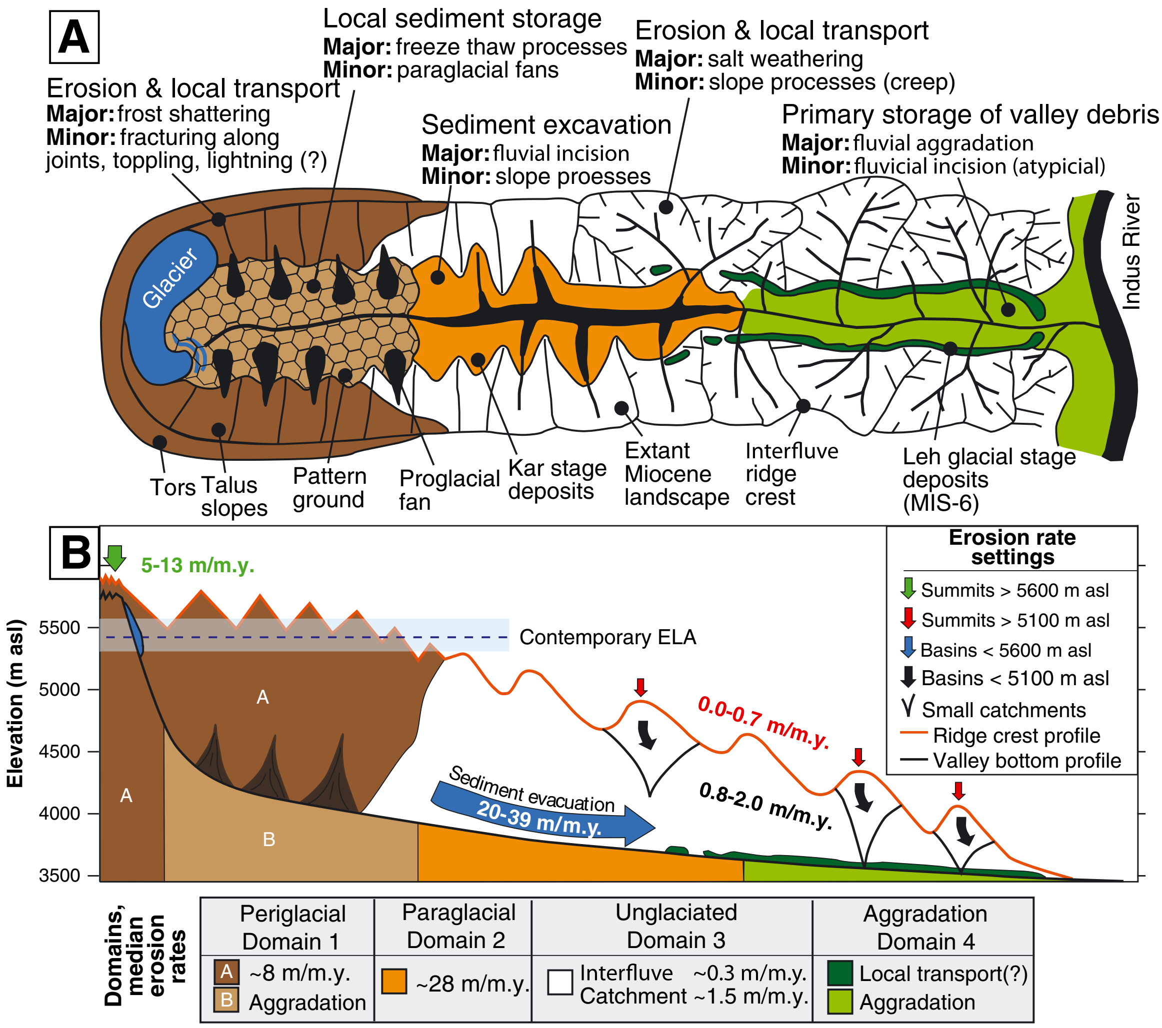

Figure 2. Schematic map (A) and cross-section (B) of morphological domains across the southwestern slope of the Ladakh Range, modified from Hobley *et al.* (2010). Map labels highlight major and minor processes of erosion and sediment transport and storage for each domain. Major geomorphic features are labeled. Black lines in (A) depict the position of streams and the terrace risers. Cross-section labels show erosion rates determined in this study and the trunk stream erosion rate of Dortch *et al.* (2011a). Vertical exaggeration is about 2.5 × . This figure is available in colour online at wileyonlinelibrary.com/journal/espl

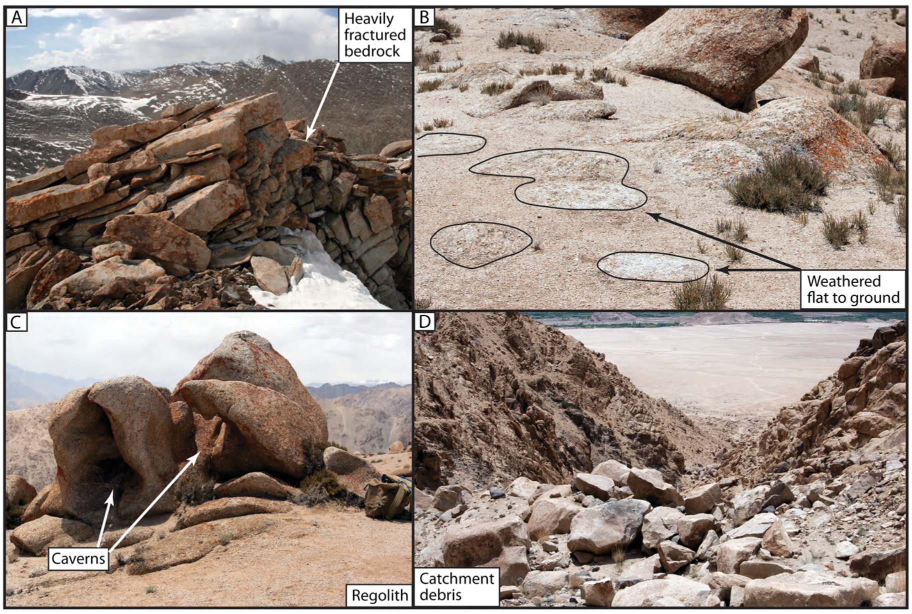

Figure 3. Views of landforms across the southwestern slope of the Ladakh Range. (A) Heavily fractured bedrock tor on the range divide at 5650 m asl in periglacial domain A (sample WL-3, Table I). Note extent of fracturing in bedrock here and the range of grain sizes. (B) and (C) Bedrock on interfluve ridge crest in the unglaciated domain with clear evidence of granular disintegration of bedrock and grussification. Note that bedrock here is weathered level to the ground surface (B) and large caverns are eroded into the undersides of small tor (C). (D) Upper reaches of a tributary catchment in the unglaciated domain choked with poorly sorted, matrix-free angular debris. This figure is available in colour online at wileyonlinelibrary.com/journal/espl

Table I. Locations for ^{10}Be TCN samples, sample sizes, topographic shielding factors, concentrations, and analytical results and ages

Sample number	Latitude (°N)	Longitude (°W)	Elevation[1] (m asl)	Depth[2] (cm)	Production rate[3] Spallation (atoms/g of SiO_2/y)	Production rate[3] Muons (atoms/g of SiO_2/y)	Shielding factor	Quartz (g)	Be carrier[4] (g)	^{10}Be/^{9}Be[5] x 10^{-13}	^{10}Be concentration[7] (10^5 atoms/g SiO_2)	^{10}Be age[9] (k.y.)	Erosion rate[10] (m/m.y.)
Summit tors on range divide													
WL-1	34.1054	77.8280	5650	4	118.65	0.879	1.000	20.1433	0.3550	73.33 ± 1.67	122.28 ± 2.79	86.4 ± 7.7	6.06 ± 0.56
WL-2	34.1053	77.8280	5649	4	118.60	0.879	1.000	20.6297	0.3489	91.75 ± 1.07	146.81 ± 1.71	103 ± 9	4.97 ± 0.45
WL-3	34.1052	77.8281	5652	4	118.75	0.880	1.000	21.2405	0.3508	64.22 ± 0.88	100.35 ± 1.38	70.3 ± 6.1	7.47 ± 0.67
NL-1	34.3608	77.3682	5634	4	118.76	0.876	1.000	20.3953	0.3515	35.63 ± 0.83	58.10 ± 1.35	40.6 ± 3.6	13.13 ± 1.17
NL-3	34.3608	77.3682	5635	4	118.81	0.877	1.000	22.1261	0.3542	56.08 ± 1.29	84.93 ± 1.96	60.0 ± 5.3	8.87 ± 0.80
Bedrock on interfluves/ridges													
CR40P	33.9672	77.7758	4098	3	57.68	0.609	1.000	21.5529	0.3571	789.10 ± 33.97	1184.52 ± 50.99	3487 ± 893	0.02 ± 0.03
CR45P	34.0107	77.7899	4566	3	72.80	0.685	1.000	13.7281	0.3550	246.60 ± 8.13	577.75 ± 19.05	775 ± 86	0.52 ± 0.08
CR50P	34.0314	77.7830	4876	2	84.28	0.745	1.000	19.0127	0.3457	407.6 ± 20.69	671.45 ± 34.08	770 ± 93	0.53 ± 0.08
LH40P	34.1782	77.6090	4053	2	56.63	0.605	1.000	6.8151	0.3552	106.20 ± 3.50	501.48 ± 16.52	871 ± 99	0.45 ± 0.07
LH45P	34.1953	77.6292	4492	1	70.54	0.683	1.000	13.1548	0.3509	362.90 ± 16.23	877.03 ± 39.22	1359 ± 186	0.23 ± 0.05
LH50P	34.2400	77.6295	5078	3	92.87	0.776	1.000	13.5029	0.3509	499.90 ± 17.74	1176.97 ± 41.77	1438 ± 192	0.21 ± 0.05
PH40P	34.1954	77.4523	4293	1	64.02	0.650	1.000	13.6031	0.3576	249.10 ± 8.29	593.28 ± 19.75	914 ± 105	0.42 ± 0.07
PH45P	34.2067	77.4617	4474	3	70.00	0.670	1.000	20.3172	0.3541	973.20 ± 40.36	1536.71 ± 63.73	4395 ± 1502	0n
PH50P	34.2344	77.4783	4998	3	89.62	0.761	1.000	15.1033	0.3557	275.80 ± 10.82	588.48 ± 23.09	609 ± 66	0.70 ± 0.09
TS40P	34.0122	77.7378	3942	1	53.27	0.593	1.000	15.4062	0.3521	613.00 ± 27.79	1269.28 ± 57.54	5837 ± 3345	0n
TS45P	34.0236	77.2697	4499	3	70.72	0.675	1.000	21.4930	0.3532	592.60 ± 21.92	882.29 ± 32.64	1396 ± 186	0.22 ± 0.05
TS50P	34.0314	77.7830	4876	3	84.28	0.739	1.000	10.7982	0.3552	297.30 ± 7.89	886.02 ± 23.51	1100 ± 130	0.32 ± 0.06
Tributary catchment sediment samples													
CR40B	33.9647	77.7839	3698	n/a[14]	n/a[14]	n/a[14]	n/a[14]	20.8835	0.3560	158.60 ± 4.88	244.95 ± 7.53	n/a[15]	1.34 ± 0.18
CR45B	33.9914	77.8011	3835	n/a[14]	n/a[14]	n/a[14]	n/a[14]	22.1386	0.3454	177.40 ± 7.88	250.76 ± 11.14	n/a[15]	1.50 ± 0.21
CR50B	34.0322	77.7981	4240	n/a[14]	n/a[14]	n/a[14]	n/a[14]	13.3057	0.3540	105.70 ± 5.74	254.78 ± 13.85	n/a[15]	1.76 ± 0.25
LH40B	34.1707	77.6041	3690	n/a[14]	n/a[14]	n/a[14]	n/a[14]	9.8387	0.3446	53.25 ± 2.39	168.98 ± 7.58	n/a[15]	1.87 ± 0.26
LH45B	34.1870	77.6232	4020	n/a[14]	n/a[14]	n/a[14]	n/a[14]	20.4073	0.3500	232.20 ± 9.83	360.80 ± 15.27	n/a[15]	1.08 ± 0.15
LH50B	34.2386	77.6195	4590	n/a[14]	n/a[14]	n/a[14]	n/a[14]	20.1980	0.3486	166.10 ± 6.17	259.73 ± 9.64	n/a[15]	1.95 ± 0.27
PH40B	34.1836	77.4586	3573	n/a[14]	n/a[14]	n/a[14]	n/a[14]	12.7289	0.3499	89.05 ± 1.99	221.78 ± 4.96	n/a[15]	1.42 ± 0.19
PH45B	34.1876	77.4680	3618	n/a[14]	n/a[14]	n/a[14]	n/a[14]	13.2696	0.3559	102.90 ± 4.40	250.04 ± 10.68	n/a[15]	1.33 ± 0.18
PH50B	34.2264	77.4872	4372	n/a[14]	n/a[14]	n/a[14]	n/a[14]	15.7561	0.3550	175.30 ± 7.46	357.84 ± 15.22	n/a[15]	1.30 ± 0.18

TS40B	34.0106	77.7256	3413	n/a[14]	n/a[14]	n/a[14]	n/a[14]	20.5068	0.3467	220.60 ± 10.30	337.90 ± 15.78	n/a[15]	0.83 ± 0.12
TS45B	34.0328	77.7622	3879	n/a[14]	n/a[14]	n/a[14]	n/a[14]	21.0646	0.3554	122.90 ± 3.79	187.86 ± 5.79	n/a[15]	2.01 ± 0.27
TS50B	34.0361	77.7578	3812	n/a[14]	n/a[14]	n/a[14]	n/a[14]	17.2378	0.3547	148.70 ± 4.12	277.22 ± 7.67	n/a[15]	1.39 ± 0.19

[1]Elevation that the samples were collected.
[2]For summit sample this is the thickness of the rock sample collected, while for basin-wide erosion sample this is the depth to which sediment was collected.
[3]Total production rate calculated for whole basin for basin-wide samples.
[4]Concentration of ^{9}Be carrier was 1.414 mg/g for samples WL-1, WL-2, WL-3, NL-1 and NL-3 and 1.354 mg/g for all other samples.
[5]Isotope ratios were normalized to ^{10}Be standards prepared by Nishiizumi *et al.* (2007) with a value of 2.85×10^{-12} and using a ^{10}Be half life of 1.36×10^{6} years.
[6]Uncertainties are reported at the 1σ confidence level.
[7]Propagated uncertainities include error in the blank, carrier mass (1%), and counting statistics.
[8]n/a Samples were corrected for a mean blank ^{10}Be/^{9}Be = $2.6 \pm 0.8 \times 10^{-15}$.
[9]Exposure age determined using time-dependent Lal (1991)/Stone (2000) scaling model calculated with the CRONUS-Earth online calculator, version 2.2 (Balco *et al.*, 2008; http://hess.ess.washington.edu/).
[10]A density of 2.7 g cm^{-3} was used for all surface samples.
[11]Propagated error in the model ages include a 6% uncertainty in the production rate of ^{10}Be and a 4% uncertainty in the ^{10}Be decay constant.
[12]Beryllium-10 erosion rates for summit boulders were calculated with the CRONUS-Earth online calculator, version 2.2 (Balco *et al.*, 2008; http://hess.ess.washington.edu/).
[13]Uncertainty includes analytical and production rate uncertainty.
n Zero erosion results reflect that the ridge crest summit samples have reached secular equilibrium between ^{10}Be production and decay, indicating a theoretical condition of zero erosion.
[14]Values are not applicable because these were intergrated across the catchement using Matlab program.
[15]Ages are not applicable because the samples are for erosion rates which are intergrated across the region and are not used to define a surface age.

differences about how they erode. Based on our field observations, granular disintegration and grussification (Figure 3(B), C)) are the dominant processes of erosion on interfluve ridges. We did not see fresh bedrock surfaces on the high-standing bedrock along interfluve bedrock ridges or any angular debris.

Tributary catchments below 5100 m asl do not contain glacial landforms; the moraines and hummocky ground produced during the last two glacial cycles present elsewhere in the Ladakh Range (Owen *et al.*, 2006; Dortch *et al.*, 2010) are absent. The hillslopes of the tributary catchments we observed are covered by relatively immobile sediment produced by granular disintegration and grussification processes. Tributary catchment hillslopes below 5100 m asl are mantled with poorly-sorted pebble and smaller size sediment. Above ~4250 m asl, tributary catchment slopes form well-defined V shapes with very little exposed bedrock. Below ~4100 m asl tributary catchment slopes are dominated by dry rills and stream channels among bedrock knobs and large, steep outcrops whose surfaces reflect intersecting joint sets. The channels of many of these lower elevation tributary catchments are filled with angular blocks without finer-grained matrix material indicating block fall, rather than landsliding, is the dominant process (Figure 3(D)). At elevations below ~4100 m asl, regolith is composed mostly of coarse quartz sand in a fine-grained matrix ('rock meal') and grus is common.

We determined rates of bedrock erosion along interfluve ridge crests that separate tributary catchments in the unglaciated domain by sampling outcrops of twelve narrow granodiorite bedrock ridges at elevations between about 3950 and 5100 m asl (Figure 4; Table I). There is no evidence of spallation, fracturing, or shattering on these bedrock ridges. Like the tor samples along the range divide, interfluve samples were collected only from bedrock standing >1 m higher than the surrounding surfaces.

We also used ^{10}Be concentrations to determine catchment-wide erosion rates for twelve small (<4 km^{2}) tributary catchments. These sampled tributary catchments bound the interfluve bedrock ridge samples making twelve summit-catchment pairs in the unglaciated domain (the CR, LH, PH, and TS sample sets of Figure 1). Catchment slopes below the interfluve ridges are 20–30°, stable, and very dry. There is minor talus development, small-scale block falls, and frost heave, suggesting that downhill mass wasting is the dominant mode of sediment mobilization and transport (Figure 3(D)). We cannot quantify the extent of sediment storage in the tributary catchments we sampled, but it is worth noting that Hobley *et al.*'s (2012) description of the intense rainstorm event in August 2010 was concentrated 4–5 km up valley from the range front and that the flooding in the lower reaches of trunk streams triggered mass flows on hillslopes in steep-sided tributary valleys. Hobley *et al.* (2012) concluded that such storms have a return period greater than 100 yr.

The paraglacial domain below ~5000 m asl (below the periglacial domain) is dominated by the trunk valley. Here, the major landforms are moraines and trunk streams are incising glacially-derived sediment. At elevations below ~3800 m asl, the lower reaches of most trunk stream valleys are filled with fluvial sediments and there is much evidence of recent aggradation. At elevations below the paraglacial domain, the tributary catchment ridges and their contiguous hillslopes, where sediment is being removed, can be readily distinguished from valley bottoms, where sediment is accumulating and well-preserved Leh glacial stage moraines are present (Owen *et al.*, 2006). Aggrading valley bottoms make up the aggradation domain.

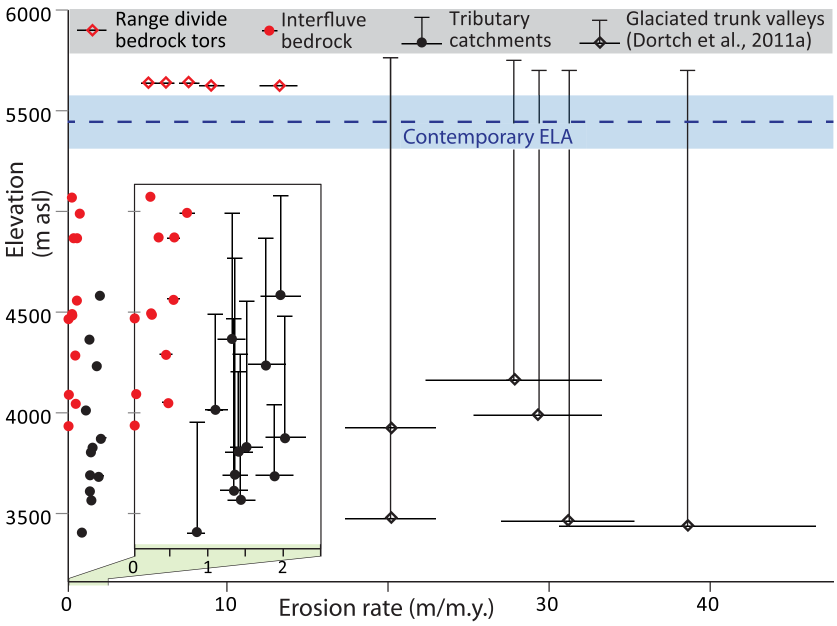

Figure 4. Erosion rates *vs.* elevation. Symbols are plotted at sample elevations determined from GPS; for catchments and trunk valleys, vertical uncertainty bars extend to their maximum elevation determined from DEMs. Horizontal lines show 1σ uncertainties for erosion rates. Inset box shows interfluve bedrock and catchment sediment samples with an expanded erosion rate scale for clarity (the y-axis is unchanged). This figure is available in colour online at wileyonlinelibrary.com/journal/espl

Analytical Methods

^{10}Be erosion rates

Cosmogenic ^{10}Be is produced primarily from cosmic rays interacting with atoms of Si and O in rocks and sediments at Earth's surface and in the crust's uppermost few meters. TCN ^{10}Be records exposure histories of these rocks and sediments as cosmic rays attenuate exponentially with depth (Lal 1988, 1991). TCN ^{10}Be concentrations within uncovered, steadily-eroding *in situ* bedrock can be used to gauge maximum bedrock erosion rates (Bierman, 1994; Small *et al.*, 1997; Bierman and Caffee, 2001; Hancock and Kirwan, 2007). Within stream sediment, TCN ^{10}Be can be used to quantify average catchment-wide erosion rates (Granger *et al.*, 1996; Portenga and Bierman, 2011 and references therein). The accuracy of catchment-wide erosion rates based on TCNs depends on the cosmic ray attenuation length, the catchment-averaged production rate, and the assumption that a particular sediment sample integrates steady-state erosional processes throughout the catchment (Bierman and Steig, 1996; Reinhardt *et al.*, 2007; Portenga and Bierman, 2011).

Quartz isolation, chemical separation of Be, and cathode preparation were completed at the University of Cincinnati (detailed in Dortch *et al.*, 2009). ^{10}Be/^{9}Be ratios were measured at the Lawrence Livermore National Laboratory (samples WL- and NL-) and the Purdue Rare Isotope Measurement Laboratory (samples CR-, LH-, PH-, and TS-). Bedrock erosion rates were calculated using the CRONUS calculator (v. 2.2; Balco, 2009). Approximately 500 g of bedrock was collected with a sample thickness between 1–5 cm at each tor sampling site along the range divide and at each bedrock sampling site along interfluvial ridges. We assessed topographic shielding for all of the bedrock samples; for tors along the range divide, topographic shielding is zero and along interfluve ridges, measured angles to the skyline were typically «20° around at least nearly half of the horizon (a constant angle of 20° produces a shielding correction factor of nearly 1 (0.98–0.97)). For our tributary catchment sediment samples, ~1 kg of sediment was collected from along a 20 m stretch of the active channel in these small basins down valley from the sampled ridge crests. Catchment-wide erosion rates were determined using the methods described in Dortch *et al.* (2011a) using MATLAB (v. 2009) code that calculates fast and slow muon production rates and corrects for topographic shielding for each pixel (90 m^2) in the catchment. Erosion rates are presented in Table I. We use a ^{10}Be sea level, high latitude production rate of 4.5 atoms g^{-1} SiO_2 y^{-1} without geomagnetic corrections following the recommendation of Owen and Dortch (2014).

Tributary catchment morphometrics

Catchment morphology (e.g. relief, mean slope, and area) can be related to erosion rate. There is a linear relationship between erosion rate and relief for large, mid-latitude drainage basins (Ahnert, 1970), but for tectonically active, high-relief mountains, the relationship is non-linear and dependent on hillslope gradient (Li, 1975; Burbank *et al.*, 1996; Hovius *et al.*, 1997; Montgomery and Brandon, 2002). To test whether our catchment-wide erosion rates could be correlated to measures of the catchments' first-order morphology, we calculated the area, maximum elevation, relief, and mean slope for the twelve small tributary catchments we sampled. To define catchments across our study area, a DEM was acquired from 3 arc-second (~90 m) SRTM data and depressions in our DEM were filled using ArcGIS 10. Flow direction and flow accumulation maps were generated and seed points correlating to sample localities were used to isolate subcatchment shapefiles. Subcatchments were extracted from SRTM DEMs, which in turn were used to calculate geomorphic statistics (maximum and minimum elevations, three-dimensional catchment area, relief, and mean slope).

Results

Calculated erosion rates of bedrock tors along the range divide vary between 5.0 ± 0.5 and 13.1 ± 1.2 m/m.y. Erosion rates of the twelve bedrock samples collected along interfluve ridge crests vary between 0 and 0.7 ± 0.1 m/m.y. (Table I, Figures 1, 2, and 4) with a median value of 0.3 m/m.y. Catchment-wide erosion rates for the twelve small tributary catchments vary between 0.8 ± 0.1 and 2 ± 0.3 m/m.y. (Table I, Figures 1, 2 and 4), with a median value of 1.4 m/m.y. Paired tributary catchment-interfluve erosion rates indicate a small amount of relief production, 0.6 ± 0.3–1.8 ± 0.3 m/m.y., but given that the erosion rate for interfluve bedrock ridges is a minimum, it is possible that the difference is even less.

Range divide tor erosion rates can be considered long-term averages over a period of 40–120 thousand years k.y. (a time average based on a cosmic ray attenuation length of 60 cm divided by the erosion rate; Lal, 1991; see also Reinhardt *et al.*, 2007). The timeframe is in accord with ^{10}Be exposure ages of the range divide samples, which range between 40–105 k.y. (Table I). The tributary catchments yield time averages for erosion of 300–750 k.y. (Lal, 1991), spanning several glacial/interglacial cycles and times of enhanced monsoon.

The relationships between catchment-wide erosion rate and catchment area, maximum elevation, relief, and mean slope for the tributary catchments we sampled in the unglaciated domain are shown in Figure 5. Erosion rates correlate most strongly with maximum elevation producing an R^2 value of 0.21 which is not significant (Figure 5(B)). Erosion rate does not correlate with catchment area, relative relief, or mean slope, as evinced by R^2 values of 0.05 or less; the weakest correlation is with relief with an R^2 of 0.01 (Figure 5(A), (C), and (D)).

Discussion

Erosion rates of range divide tors and 'tor cycling'

Erosion rates between 5 and 13 m/m.y. of tors between 5600 and 5700 m asl along the range divide are typical of granitic bedrock from alpine regions across the world, e.g., 6-8 m/m.y. (Small *et al.*, 1997; Lal *et al.*, 2003; Hancock and Kirwan, 2007). Soil-mantled granites in the Swiss Alps eroded at similar rates (Norton *et al.*, 2010) but soil-mantled slopes from the western Sierra Nevada erode twice as fast (Dixon *et al.*, 2009). The erosion rates of range divide tors are minimum values for the lowering of range divide bedrock. Erosion of range divide tors by block removal and shattering is not a steady-state process. Models of episodic (step-wise) erosion of bedrock summit surfaces (Lal, 1991; Small *et al.*, 1997) suggest the mean of several measured erosion rates from different tors can provide a good estimate of the actual, long-term average erosion rate, especially in cases that have a high frequency of erosional variation (Heimsath, 2006).

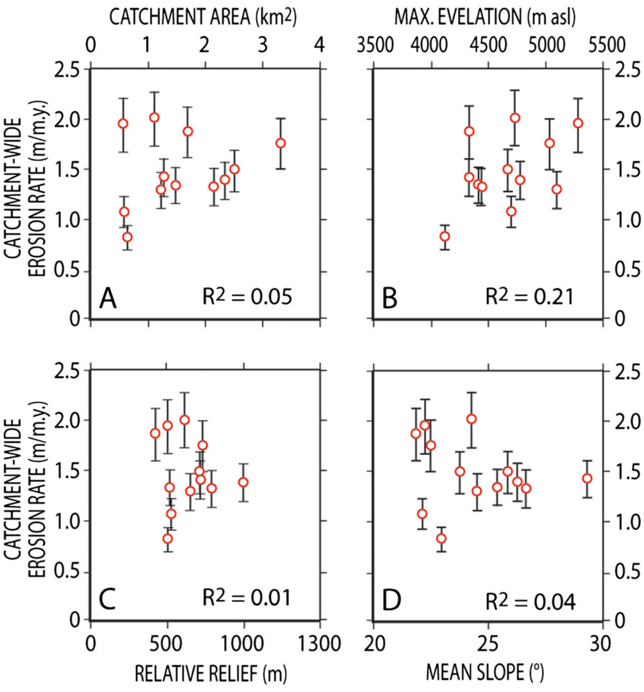

Figure 5. Catchment-wide erosion rate versus (A) catchment area, (B) maximum elevation, (C) relative relief, and (D) mean slope for tributary catchments in the unglaciated domain. This figure is available in colour online at wileyonlinelibrary.com/journal/espl

To gain a better understanding of how tor fields develop with the cycling of individual tors through time, we took the tor with the highest ^{10}Be concentration and assumed that this tor represents the end-stage of tor development; tors with lower ^{10}Be concentrations have been eroded. The thickness of material lost, assuming loss occurred instantaneously, can be estimated by evaluating measured ^{10}Be concentrations along a model ^{10}Be production curve, that is, as if they were sampled at depth. By normalizing ^{10}Be concentrations, the effects of differential shielding among different sampled tors that may have occurred even though samples are at similar elevations and share the same geographic and geologic setting are limited. Normalized ^{10}Be concentrations plotted on a ^{10}Be production curve that assumes homogeneous lithology (granite) with density of 2.7 g/cm^3 (Figure 6(A)) can be translated to depth assuming an e-folding length of 60 cm. The timing of instantaneous thickness loss can be estimated by taking the difference in ^{10}Be concentration compared to the tor with the highest concentration and calculating an age (Figure 6(B)). Results suggest ~11–56 cm of loss occurring over 20–80 k.y., with an average of ~24 cm lost instantaneously every ~40 k.y. The timescale of 10^4 years is at the lower end of the long-term average period (40–120 k.y.) over which the 5–13 m/m.y. erosion rates have occurred. These calculations define the time frame during which new range divide ridges develop a tor morphology, that is, the rate of 'tor cycling' as the range divide changes position through cirque headwall erosion. The short duration of 'tor erosion' (20–80 k.y.) suggests that there is an initial 20–40 k.y. period during which tors first develop on a landscape and remain relatively stable (episodically losing thickness) during the cycling process. A range divide may move laterally due to glacial headwall erosion and develop a new tor field with a dynamic range of ages on a lower elevation bedrock ridge within a 10^5 yr timeframe. Indeed as shown on Figure 1, the range divide is discontinuous where it has been eroded through in several places, becoming a valley bottom instead of a ridge of tors. Lowering the divide results in a negative feedback as gravitational potential is lowered and slope angle is decreased in concordance with maximum elevation, which, in turn, reduces the rate of headwall collapse by glacial over steepening.

Processes of erosion of range divide tors

Talus slopes comprise the vast majority of sediment along the range divide in periglacial domain A and fracturing along joints, block toppling, and exfoliation are important in conditioning bedrock for shattering into pebble-sized and larger grains. Hales and Roering (2007, 2009) showed that rock fracture by ice growth is most intense at elevations where the mean annual temperature (MAT) is just above 0 °C and where rock temperature is just below 0 °C; frost shattering by the growth of segregation ice is most efficient within a temperature range of –3 to –8 °C. The modern 0 °C MAT of the Ladakh Range is ~4300 m asl, below where talus-mantled hillslopes occur. More recently, Girard *et al.* (2013) conducted an *in situ*

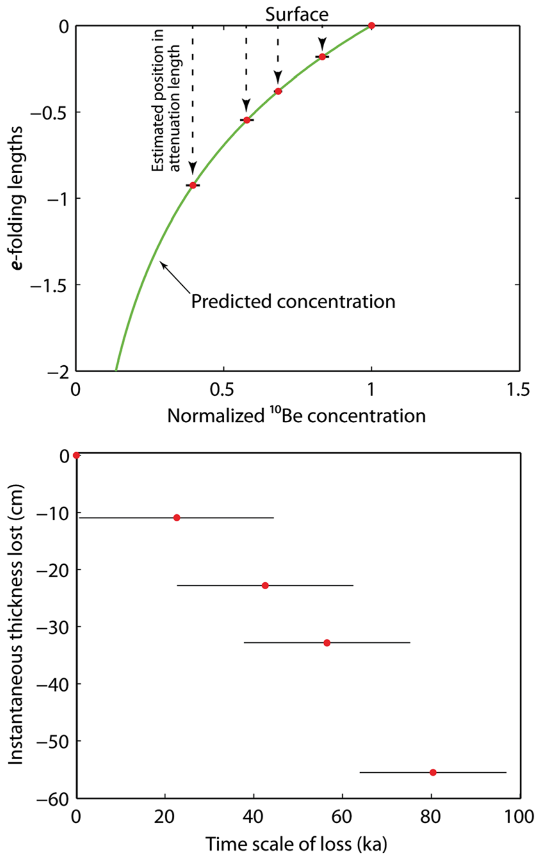

Figure 6. (A) Normalized ^{10}Be concentrations of range divide tors plotted on a ^{10}Be production curve as if they were sampled at depth. The production curve assumes homogeneous granite lithology with a density of 2.7 g/cm^3 and the curve is translated to depth assuming an e-folding length of 60 cm. Uncertainty bars are 1-σ of the normalized concentrations. (B) Instantaneous thickness loss of range divide tors versus time scale of loss; see text for discussion. Uncertainty bars represent internal uncertainty from the CRONUS calculator (version 2.2) at 1-σ, propagated additively to account for both samples when comparing their differences in ^{10}Be concentration. Internal uncertainties are used since external errors would unjustifiably increase uncertainty. All tor samples are from the same region of the range divide and were collected at similar elevation and latitude so these effects on scaling differences are negligible. This figure is available in colour online at wileyonlinelibrary.com/journal/espl

study of frost cracking by measuring acoustic emissions (as a proxy for cracking), temperature, and water content in fractured bedrock in the central Swiss Alps at an elevation of 3500 m asl. Girard *et al.* (2013) concluded that sustained freezing can yield much stronger frost cracking than repeated freezing and thawing cycles, but frost cracking can occur even during short periods of freezing and even under relatively dry near-surface conditions.

Using temperature data collected at Leh (Weatherbase.com, 2013) and a lapse rate of 6.4 °C/km (Anderson and Anderson, 2010), the average temperature of the highest sample along the range divide (5652 m als) is –8.8 °C, with an average temperature for the months December through March of –19.5 °C. December through March was the interval of the lowest sustained sub-zero temperatures measured by Girard *et al.* (2013), reaching a minimum of –15 °C at a depth of 50 cm in February, and the interval with the highest and most sustained acoustic emission energy. From Girard *et al.*'s (2013) *in situ* data and measured temperatures in Leh extrapolated to the range divide, we propose that frost shattering reaches depths of 5–10 cm after the warm summer months of July and August, and advances to depths of at least 50 cm or greater during the winter months, even extending into April. The depth of frost shattering returns to the surface by summer. This depth of cracking/shattering is in agreement with our thickness loss estimated from ^{10}Be concentrations.

Lightning is another explanation for bedrock shattering, which can crack and move bedrock. Anderson *et al.* (2006) estimated that 20–30 lightning strikes/y/km^2 along the summit of the Laramide Front Range could produce an erosion rate of 20 m/m.y. Using field evidence related to the degree of surface weathering and patterns of fractures, significant erosion by lightning on mountain summits has also been proposed in South Africa (Knight and Grab, 2014). The Lightning Imaging Sensor from TRMM has recorded ~20–30 lightning flashes per km^2 over the Ladakh Range from April–November 1999 (Barros *et al.*, 2004). While many of these flashes may not have reached ground, it is possible for lightning strikes to have contributed to the divide erosion rates. Even though distinguishing angular bedrock debris produced by lightening strikes versus frost shattering or other climate-modulated processes is not clear-cut, we accordingly include lightning as a minor erosional process in periglacial domain A (Figure 2).

Erosion rates in the unglaciated domain

Erosion rates of the twelve bedrock ridge interfluve samples we collected at elevations between 3900 and 5100 m asl in the unglaciated domain vary between 0 and ≤0.7 ± 0.1 m/m.y.; these are minimum values. These rates are among the lowest determined by TCN methods anywhere on Earth (Portenga and Bierman, 2011) and are similar to those found in the low-relief deserts of Namibia (Bierman and Caffee, 2001), Australia (Bierman and Turner, 1995; Bierman and Caffee, 2002), the Near East (Matmon *et al.*, 2009) and the Atacama (Nishiizumi *et al.*, 2005; Kober *et al.*, 2007). Erosion rates of mountainous bedrock slopes from semi-arid central Australia are more than twice as fast, 1.5–1.8 m/m.y. (Heimsath *et al.*, 2010). Interfluve bedrock samples yield time averages for erosion of >850 k.y. (Lal, 1991) and their ^{10}Be ages are >600 k.y. (Table I). Based on our field observations of granular disintegration, chemical weathering and grusification is the dominant form of erosion on tributary interfluve ridges at elevations below 5100 m asl. The lack of fresh bedrock surfaces along tributary catchment ridges and the accumulation of grus suggests that limited sediment transport contributes to slow bedrock erosion. Erosion rates of bedrock ridge interfluve samples are an order-of-magnitude lower than bedrock tor samples along the range divide. Field observations show that as elevation decreases, frost processes decline in relative importance compared with granular disintegration, likely due to declining average precipitation at lower elevations. Calculated bedrock erosion rates in the unglaciated domain provide evidence that the southwestern slope of the Ladakh Range, at least where we have sampled, has received very little precipitation since the Leh glacial stage.

The twelve tributary catchments in the unglaciated domain yield erosion rates between 0.8 ± 0.1 and 2.0 ± 0.3 m/m.y. Slow erosion rates might be expected in these small (<4 km^2) tributary catchments given their mean slopes and relative relief (Figure 5; Montgomery and Brandon, 2002) but these tributary catchments are typical of the unglaciated domain. In addition, the differences between the largest and smallest values of catchment area (3 km^2), maximum elevation (1150 m), relief (600 m), and mean slope (7°) may also be too small to capture potential correlations with erosion rate (Figure 5).

Niemi *et al.* (2005) modeled erosion rates in catchments where erosion is dominated by landslides including small catchments similar to those we sampled, and the rate of landsliding scales with catchment size. Niemi *et al.* (2005)

showed that TCNs in sediment samples statistically represent the total volumetric erosion rate including landslides on timescales of 10^3 to 10^4 y. Niemi *et al.* (2005) also concluded that sampling several similarly-sized catchments, even where landslides are active, will likely yield samples whose TCN-derived erosion rates accurately reflect the catchments' total volumetric erosion rate for timescales of 10^4 yr. Cavernous boulders and rock meal record the dominant form of weathering in the unglaciated domain, and grus occurs as a thin surface layer, features consistent with salt weathering (Wellman and Wilson, 1965). If bedrock mass movements of any scale affected the arid interfluve ridges, angular debris and bedrock scars would be visible and preserved but they are not. Tectonic quiescence and fluvial aggradation have conspired to stabilize slopes, decreasing the potential for landsliding through time. From these results, we conclude that individual erosion rates of the interfluve bedrock samples are minimum bedrock rates (Niemi *et al.*, 2005) and that for a timescale of 10^5 y, the average of the bedrock erosion rates capture stochastic processes and yield reliable results (Small *et al.*, 1997).

Based on our paired tributary catchment-interfluve erosion rates, the maximum increase in relief in the unglaciated domain is 1.8 ± 0.3 m/m.y. At lower elevations below the Leh glacial stage ELA, extensive aggradation along trunk streams (Hobley *et al.*, 2010; Figure 2) in the aggradation domain indicates that alluviation is destroying relief. The slightly higher erosion rate of the tributary catchments may reflect the erosive work of infrequent monsoonal storms that increase the rate of creep.

The role of glacial conditioning and landscape preservation

Along the southwestern slope of the Ladakh Range, erosion rates measured in stream sediments depend on glacial history. Erosion rates for three trunk streams in the paraglacial domain measured by Dortch *et al.* (2011a) are 20–40 m/m.y., at least 10–20 times greater than the unglaciated tributary catchments (Figures 1, 2 and 4), but these rates are still slow. Two of these trunk streams were sampled at different elevations including higher elevations in areas more recently glaciated (Figure 1). Erosion rates calculated for individual samples in both catchments were within 1σ uncertainty of each other (Dortch *et al.*, 2011a), indicating that erosion is relatively uniform without a significant component of inherited sediment. Glacial and fluvial processes in trunk valleys at elevations >5100 m asl are much more effective drivers of erosion and sediment evacuation, respectively, than hillslope processes that dominate the smaller tributary catchments. Glaciers conditioned high altitude hillslopes between 5100 and 5600 m asl by producing over-steepened slopes and generating the sediment delivered further down valley by trunk streams. However, trunk streams are generally insulated from the deposits in both of the periglacial domains due to very limited sediment transport. Talus slopes and periglacial fans form but are not fluvially incised. The difference in erosion rates between range summit tors and glaciated catchments along the Ladakh Range's southwestern slope show that relief is increasing across the paraglacial domain as trunk streams incise moraines, the primary source of sediment that is being evacuated from the range. But erosion by trunk streams is still at least 10–20 times slower than long-term (10^7 yr) exhumation rates of 400–750 m/m.y. derived from modeling of apatite and zircon helium and fission-track thermochronologic data by Kirstein *et al.* (2009).

Tripathy-Lang *et al.* (2013) calculated a long-term, time-averaged erosion rate for a single catchment along the southwestern slope of the Ladakh Range using laser ablation (U-Th)/He age data from a river sand detrital zircon population and the modeling approach of Brandon *et al.* (1998). Their modeled erosion rate was 430 m/m.y., at least ten times higher than the rate for trunk streams traversing the paraglacial domain. Tripathy-Lang *et al.* (2013) suggest that there was a significant reduction in erosion rate during the Neogene. A pronounced decrease in erosion rate is consistent with our erosion rate data that show that three of four domains do not significantly contribute to sediment evacuation. Catchment erosion rates reported by Dortch *et al.* (2011a) recalculated to only include the paraglacial domain would be ~30% lower due to a lower average ^{10}Be production rate. In addition, the duration recorded by our TCN-derived erosion rates is likely on the order of $10^{4\text{-}6}$ y (Lal, 1991; Dortch *et al.*, 2011a) when considering the inheritance memory down to 10 folding depths (cf. Parker and Perg, 2005), indicating that the sediment contribution of the unglaciated tributary catchments to their trunk streams has been negligible since perhaps the Late Miocene to Pliocene (7.5−2 Ma). Our very slow erosion data also support ELA reconstructions (Figure 1) that show tributary catchments have not been affected by glaciation since at least ~300 ka, the age of Leh glacial stage. We attribute the preservation of this landscape to a sustained arid environment. By synthesizing results related to the ages and rates of erosion and exhumation (Dortch *et al.*, 2011a, 2013; Kirstein, 2011; Tripathy-Lang *et al.*, 2013), we speculate that the decrease in the rates of erosion in the Ladakh Range during the Neogene may have been initiated by a decrease in monsoon influence due to continued uplift of the Greater Himalaya (Catlos *et al.*, 2001; Wobus *et al.*, 2005). This view is supported by cores from the Bengal fan where major uplift and erosion between 7.5–10.9 Ma is recorded mineralogically with a subsequent decrease in pumpellyite sourced from the upper Indus basin (Amano and Taira, 1992) and where argon cooling ages record episodic uplift of the southern slope of the Himalaya beginning in the late Miocene (Copeland and Harrison, 1990).

Conclusions

Denudation of the southwestern slope of the Ladakh Range is taking place across a network of geomorphic domains, each with a characteristic erosion rate and dominant erosional process, and each affected differently by Pleistocene glaciation. High-glaciated basins and frost-weathered bedrock in the periglacial domain above the lowest ELA in the past ~300 ka denude at rates that are up to an order of magnitude faster than their lower elevation, unglaciated counterparts. Periglacial talus slopes that extend as high as 5400 m asl are derived from frost shattered tors along the range divide. Tors between 5600 and 5700 m asl along the range divide are eroding between 5.0 ± 0.5 and 13.1 ± 1.2 m/m.y. The tors and their talus slopes have likely persisted in the landscape for 40 ka or longer but they will eventually be moved southwards as glacial headwall erosion from north-side glaciers changes the position of the range divide. Tributary catchments below 5100 m asl were not glaciated during the Leh glacial stage and are eroding extremely slowly, <2 m/m.y.; bedrock along their influvial ridge crests is eroding even more slowly, $\leq 0.7 \pm 0.1$ m/m.y. This unglaciated domain represents an extant landscape ($10^{5\text{-}6}$ k.y.) at least one order, and perhaps two orders of magnitude older than the periglacial domains.

Rates of tectonically-driven exhumation in the Ladakh Range (Kirstein *et al.*, 2009; Tripathy-Lang *et al.*, 2013) were at least ten times faster than the fastest, post-tectonic erosion rate. Following cessation of tectonic uplift in the Miocene, an overall hierarchy of erosion rates appears to have been achieved, governed by the extent of glaciation. In the upper reaches of glaciated valleys, fluvial incision of glacial debris in trunk streams is about ten times faster than erosion driven by periglacial processes along the range divide and its high elevation slopes, which in turn is about ten times faster than bedrock erosion in unglaciated tributary catchments and along their interfluvial bedrock ridges. To drive the much faster Miocene exhumation of the Ladakh Range, we suggest three possibilities: the current set of erosional processes scaled to much faster rates (Zeitler, 2014), the boundary of the periglacial and paraglacial domains was shifted significantly down valley in addition to scaled rates of erosion, or a different set of erosional processes was governing landscape evolution during tectonic uplift.

Acknowledgements—SAR thanks the Geological Society of America for the Arthur D. Howard Award for supporting this study during his M.S. project, which contributed to this paper. LAO thanks NSF award EAR-0910759 for funding the ^{10} Be analyses. We thank Susan Ma (PRIME Lab) for technical support. Jason Barnes, Arjun Heimsath, and Josh Roering provided insightful reviews that significantly improved the manuscript. Thorough reviews by Dan Hobley and two anonymous reviewers improved an earlier version of it. Helpful editorial support was provided by Fiona Kirkby. The expert assistance of Tsewang Dorje (Discover Ladakh Adventure), Tenzin Bhun Sen Bodh, Lotum, and Kilte made fieldwork possible. For JMD and SAR, fieldwork was greatly assisted by the power of Royal Enfield motorcycles. CD and LAO gratefully acknowledge the support of the University of Cincinnati International Programs Office.

References

Adams B, Dietsch C, Owen LA, Caffee MW, Spotila J, Haneberg WC. 2009. Exhumation and incision history of the Lahul Himalaya, northern India, based on (U-Th)/He thermochronometry and terrestrial cosmogenic nuclide methods. *Geomorphology* **107**: 285–299.

Ahnert F. 1970. Functional relationships between denudation, relief, and uplift in large md-latitude drainage basins. *American Journal of Science* **268**: 243–263.

Amano K, Taira A. 1992. Two-phase uplift of Higher Himalayas since 17 Ma. *Geology* **20**: 391–394.

Anders AM, Roe GH, Hallet B, Montgomery DR, Finnegan NJ, Putkonen J. 2006. Spatial patterns of precipitation and topography in the Himalaya. *Geological Society of America, Special Paper* **398**: 39–53. DOI: 10.1130/2006.2398(03)

Anderson RS. 2002. Modeling the tor-dotted crests, bedrock edges, and parabolic profiles of high alpine surfaces of the Wind River Range, Wyoming. *Geomorphology* **46**: 35–58.

Anderson RS. 2005. Teflon peaks: the evolution of high local relief in glaciated mountain ranges. *Eos, Transactions American Geophysical Union* **86**(52): Fall Meet. Suppl., Abstract H33F-04.

Anderson RS, Anderson SP. 2010. *Geomorphology: The Mechanics and Chemistry of Landscapes*. Cambridge University Press: Cambridge.

Anderson RS, Riihimaki CA, Safran EB, MacGregor KR. 2006. Facing reality: Late Cenozoic evolution of smooth peaks, glacially ornamented valleys, and deep river gorges of Colorado's Front Range. In *Tectonics Climate, and Landscape Evolution,* Willett SD, Hovius N, Brandon MT, Fisher DM (eds). Geological Society of America: Boulder, Geological Society of America Special Paper, **398**: 397–418.

Balco G. 2009. 26Al–10Be exposure age/erosion rate calculators: update from v.2.1 to v. 2.2. http://hess.ess.washington.edu/math/docs/al_be_v22/AlBe_changes_v22.pdf [Accessed 16 November 2013].

Balco G, Briner J, Finkel RC, Rayburn J, Ridge JC, Schaefer JM. 2008. Regional beryllium-10 production rate calibration for late-glacial northeastern North America. *Quaternary Science Reviews* **4**: 93–107.

Barros AP, Kim G, Williams E, Nesbitt SW. 2004. Probing orographic controls in the Himalayas during the monsoon using satellite imagery. *Natural Hazards and Earth System Sciences* **4**: 29–51.

Benn DI, Owen LA. 1998. The role of the Indian summer monsoon and the midlatitude westerlies in Himalayan glaciation; review and speculative discussion. *Journal of the Geological Society of London* **155**: 353–363.

Berger AL, Spotila JA. 2008. Denudation and deformation of a glaciated orogenic wedge: the St. Elias orogen Alaska. *Geology* **36**: 523–526.

Bierman PR. 1994. Using in situ cosmogenic isotopes to estimate rates of landscape evolution: a review from the geomorphic perspective. *Journal of Geophysical Research* **99**: 13885–13896.

Bierman PR, Turner J. 1995. ^{10}Be and ^{26}Al evidence for exceptionally low rates of Australian bedrock erosion and the likely existence of pre-Pleistocene landscapes. *Quaternary Research* **44**: 378–382.

Bierman PR, Steig E. 1996. Estimating rates of denudation and sediment transport using cosmogenic isotope abundances in sediment. *Earth Surface Processes and Landforms* **21**: 125–139.

Bierman PR, Caffee M. 2001. Slow rates of rock surface erosion and sediment production across the Namib Desert and escarpment, southwestern Africa. *American Journal of Science* **301**: 326–358.

Bierman PR, Caffee M. 2002. Cosmogenic exposure and erosion history of Australian bedrock landforms. *Geological Society of America Bulletin* **114**: 787–803.

Bookhagen B, Thiede RC, Strecker MR. 2005. Abnormal monsoon years and their control on erosion and sediment flux in the high, arid northwest Himalaya. *Earth and Planetary Science Letters* **231**: 131–146.

Bookhagen B, Burbank DW. 2006. Topography, relief, and TRMM-derived rainfall variations along the Himalaya. *Geophysical Research Letters* **33**: L08405. DOI: 10.1029/2006GL26037

Brandon MT, Roden-Tice MK, Garver JI. 1998. Late Cenozoic exhumation of the Cascadia accretionary wedge in the Olympic Mountains, northwest Washington State. *Geological Society of America Bulletin* **110**: 985–1009.

Brown ET, Bendick R, Bourles DL, Gaur V, Molnar P, Raisbeck GM, Yiou F. 2002. Slip rates of the Karakoram fault, Ladakh, India, determined determined using cosmic ray exposure dating of debris flows and moraines. *Journal of Geophysical Research* **107**: DOI: 10.1029/2000JB000100

Brozović N, Burbank DW, Meigs AJ. 1997. Climatic limits on landscape development in the northwestern Himalaya. *Science* **276**: 571–574.

Burbank DW, Fort MB. 1985. Bedrock control on glacial limits; examples from the Ladakh and Zanskar Ranges, north-western Himalaya. *Journal of Glaciology* **31**: 143–149.

Burbank DW, Leland J, Fielding E, Anderson RS, Brozovic N, Reid MR, Duncan C. 1996. Bedrock incision, rock uplift and threshold hillslopes in the northwestern Himalayas. *Nature* **379**: 505–510.

Catlos EJ, Harrison TM, Kohn MJ, Grove M, Ryerson FJ, Manning CE, Upreti BN. 2001. Geochronologic and thermobarometric constraints on the evolution of the Main Central Thrust, central Nepal Himalaya. *Journal of Geophysical Research* **106**: 16177–16204.

Chevalier M-L, Ryerson FJ, Tapponnier P, Finkel RC, Van Der Woerd J, Haibing L, Qing L. 2005. Slip-rate measurements on the Karakoram Fault may imply secular variations in fault motion. *Science* **307**: 411–414.

Copeland P, Harrison MT. 1990. Episodic rapid uplift in the Himalaya revealed by ^{40}Ar/^{39}Ar analysis of detrital K-feldspar and muscovite, Bengal fan. *Geology* **18**: 353–357.

Dixon JL, Heimsath AM, Kaste J, Amundson R. 2009. Climate-driven processes of hillslope weathering. *Geology* **37**: 975–978.

Dortch JM, Owen LA, Caffee MW. 2009. Late Quaternary glaciation and ELA variations of the McKinley River region, central Alaska Range. *Boreas* **39**: 233–246.

Dortch JM, Owen LA, Caffee MW. 2010. Quaternary glaciation in the Nubra and Shyok valley confluence, northernmost Ladakh, India. *Quaternary Research* **74**: 132–144.

Dortch JM, Owen LA, Schoenbohm LM, Caffee MW. 2011a. Asymmetrical erosion and morphological development of the central Ladakh Range, northern India. *Geomorphology* **135**: 167–180.

Dortch JM, Dietsch C, Owen LA, Caffee MW, Ruppert K. 2011b. Episodic fluvial incision of rivers and rock uplift in the Himalaya and Transhimalaya. *Journal of the Geological Society, London* **168**: 783–804.

Dortch JM, Owen LA, Caffee MW. 2013. Timing and climatic drivers for glaciation across semi-arid western Himalayan-Tibetan orogeny. *Quaternary Science Reviews* **78**: 188–208.

Egholm DL, Nielsen SB, Pedersen VK, Leseman J-E. 2009. Glacial effects limiting mountain height. *Nature* **460**: 884–888.

Finnegan NJ, Hallet B, Montgomery DR, Zeitler PK, Stone JO, Anders AM, Yuping L. 2008. Coupling of rock uplift and river incision in the Namche Barwa-Gyala Peri massif, Tibet. *Geological Society of America Bulletin* **120**: 142–155.

Fort M. 1983. Geomorphological observations in the Ladakh area (Himalayas): Quaternary evolution and present dynamics. In *Stratigraphy and Structure of Kashmir and Ladakh, Himalaya*. Gupta VJ (ed). Hindustan Publishing: New Delhi; 39–58.

Gasse F, Fontes JC, van Campo E, Wei K. 1996. Holocene environmental changes in Bangong Co basin (western Tibet): Part 4: discussion and conclusions. *Paleogeography, Paleoclimatology, Paleoecology* **120**: 79–92.

Girard L, Gruber S, Weber S, Beutel J. 2013. Environmental controls of frost cracking revealed through *in situ* acoustic emission measurements in steep bedrock. *Geophysical Research Letters* **40** 1748–1753. DOI: 10.1002/grl.50384

Godard V, Lave J, Cattin R. 2006. Numerical modelling of erosion processes in the Himalaya of Nepal: Effects of spatial variation of rock strength and precipitation. In *Analogue and Numerical Modelling of Crustal-Scale Processes*, Buiter SJH, Schreurs G (eds). Geological Society of London: London; 341–358.

Godin L, Grujic D, Law RD, Searle MP. 2006. Channel flow, ductile extrusion and exhumation in continental collision zones: an introduction. In *Channel Flow, Ductile Extrusion and Exhumation in Continental Collision Zones*. Law RD, Searle MP, Godin L (eds). The Geological Society: London; 1–23.

Granger DE, Kirchner JW, Finkel R. 1996. Spatially averaged long-term erosion rates measured from in situ-produced cosmogenic nuclides in alluvial sediment. *Journal of Geology* **104**: 249–257.

Hales TC, Roering JJ. 2007. Climatic controls on frost cracking and implications for the evolution of bedrock landscapes. *Journal of Geophysical Research* **112**: F02033. DOI: 10.1029/2006JF000616

Hales TC, Roering JJ. 2009. A frost 'buzz-saw' mechanism for erosion of the eastern Southwestern Alps, New Zealand. *Geomorphology* **107**: 241–253.

Hancock G, Kirwan M. 2007. Summit erosion rates deduced from ^{10}Be: implications for relief production in the central Appalachians. *Geology* **35**: 89–92.

Harris N. 2007. Channel flow and the Himalayan–Tibetan orogen: a critical review. *Journal of the Geological Society* **164**: 511–523.

Hedrick KA, Seong YB, Owen LA, Caffee MC, Dietsch C. 2011. Towards defining the transition in style and timing of Quaternary glaciation between the monsoon-influenced Greater Himalaya and the semi-arid Transhimalaya of Northern India. *Quaternary International* **236**: 21–33.

Heimsath A. 2006. Eroding the land: Steady-state and stochastic rates and processes through a cosmogenic lens. In *In Situ-Produced Cosmogenic Nuclides and Quantification of Geological Processes*, Siame LI, Bourlès DL, Brown ET (eds). Geological Society of America: Boulder, Geological Society of America Special Paper **415**: 111–129. DOI: 10.1130/2006.2415(07)

Heimsath AM, Chappell J, Fifield K. 2010. Eroding Australia: rates and processes from Bega Valley to Arnhem Land. In *Australian Landscapes*. Bishop P, Pillans B (eds). The Geological Society: London, Special Publications **346**: 225–241.

Hobley DEJ, Sinclair HD, Cowie PA. 2010. Processes, rates, and time scales of fluvial response in an ancient postglacial landscape of the northwest Indian Himalaya. *Geological Society of America Bulletin* **122**: 1569–1584.

Hobley DEJ, Sinclair HD, Mudd SM. 2012. Reconstruction of a major storm event from its geomorphic signature: the Ladakh floods, 6 August 2010. *Geology* **40**: 483–486.

Hovius N, Stark CP, Allen PA. 1997. Sediment flux from a mountain belt derived by landslide mapping. *Geology* **25**: 231–234.

Huntington KW, Blythe AE, Hodges KV. 2006. Climate change and Late Pliocene acceleration of erosion in the Himalaya. *Earth and Planetary Science Letters* **252**: 107–118.

Jamieson SSR, Sinclair HD, Kirstein LA, Purves RS. 2004. Tectonic forcing of longitudinal valleys in the Himalaya: morphological analysis of the Ladakh batholith. N. India. *Geomorphology* **58**: 49–65.

Kaplan MR, Hein AS, Hubbard A, Lax SM. 2009. Can glacial erosion limit the extent of glaciation? *Geomorphology* **103**: 172–179.

Kirstein LA, Sinclair H, Stuart FM, Dobson K. 2006 Rapid early Miocene exhumation of the Ladakh batholith, western Himalaya. *Geology* **34**: 1049–1052.

Kirstein LA, Foeken JPT, van der Beek P, Stuart FM, Phillips RJ. 2009. Cenozoic unroofing history of the Ladakh batholith, western Himalaya, constrained by thermochronology and numerical modeling. *Geological Society of London* **166**: 667–678.

Kirstein LA. 2011. Thermal evolution and exhumation of the Ladakh batholith, northwest Himalaya, India. *Tectonophysics* **503**: 222–233.

Knight J, Grab SW. 2014. Lightning as a geomorphic agent on mountain summits: evidence from southern Africa. *Geomorphology* **204**: 61–70.

Kober F, Ivy-Ochs S, Schlunegger F, Baur H, Kubik PW, Wieler R. 2007. Denudation rates and a topography-driven rainfall threshold in northern Chile: multiple cosmogenic nuclide data and sediment yield budgets. *Geomorphology* **83**: 97–120.

Korup O, Montgomery DR. 2008. Tibetan plateau river incision inhibited by glacial stabilization of the Tsangpo gorge. *Nature* **455**: 786–789.

Kumar R, Lal N, Singh S, Jain AK. 2007. Cooling and exhumation of the Trans-Himalayan Ladakh batholith as constrained by fission track apatite and zircon ages. *Current Science* **92**: 490–496.

Lal D. 1988. In-situ-produced cosmogenic isotopes in terrestrial rocks. *Annual Review of Earth and Planetary Sciences* **16**: 355–388.

Lal D. 1991. Cosmic ray labeling of erosion surfaces: in situ nuclide production rates and erosion models. *Earth and Planetary Science Letters* **104**: 424–439.

Lal D, Harris NBW, Sharma KK, Gu Z, Ding L, Liu T, Dong W, Caffee MW, Jull AJT. 2003. Erosion history of the Tibetan Plateau since the last interglacial: constraints from the studies of cosmogenic ^{10}Be from Tibetan bedrock. *Earth and Planetary Science Letters* **217**: 33–42.

Lavé J, Avouac JP. 2001. Fluvial incision and tectonic uplift across the Himalayas of central Nepal. *Journal of Geophysical Research* **106** (B11): 26561–26591.

Leland J, Reid MR, Burbank D, Finkel R, Caffee M. 1998. Incision and differential bedrock uplift along the Indus River near Nanga Parbat, Pakistan Himalaya, from ^{10}Be and ^{26}Al exposure age dating of bedrock straths. *Earth and Planetary Science Letters* **154**: 93–107.

Li YH. 1975. Denudation of Taiwan island since the Pliocene epoch. *Geology* **4**: 105–107.

Matmon A, Simhai O, Amit R, Haviv I, Porat N, McDonald E, Benedetti L, Finkel R. 2009. Desert pavement – coated surfaces in extreme deserts present the longest-lived landforms on Earth. *Geological Society of America Bulletin* **121**: 688–697.

Mitchell SG, Montgomery DR. 2006. Influence of a glacial buzzsaw on the height and morphology of the Cascade Range in central Washington State, USA. *Quaternary Research* **65**: 96–107.

Montgomery DR. 1994. Valley incision and the uplift of mountain peaks. *Journal of Geophysical Research* **99**(B7): 13913–13921.

Montgomery DR, Balco G, Willett SD. 2001. Climate, tectonics, and the morphology of the Andes. *Geology* **29**: 579–582.

Montgomery DR, Brandon MT. 2002. Topographic controls on erosion rates in tectonically active mountain ranges. *Earth and Planetary Science Letters* **201**: 481–489.

Murari MK, Owen LA, Dortch JM, Caffee MW, Dietsch C, Fuchs M, Haneberg WC, Sharma MC, Townsend-Small A. 2014. Timing and climatic drivers for glaciation across monsoon-influenced regions of the Himalayan-Tibetan orogen. *Quaternary Science Reviews* **88**: 159–182.

Niemi NA, Oskin M, Burbank DW, Heismath AM, Gabet EJ. 2005. Effects of bedrock landslides on cosmogenically determined erosion rates. *Earth and Planetary Science Letters* **237**: 480–498.

Nishiizumi K, Caffee M, Finkel R, Brimhall G, Mote T. 2005. Remnants of a fossil alluvial fan landscape of Miocene age in the Atacama Desert of northern Chile using cosmogenic nuclide exposure age dating. *Earth and Planetary Science Letters* **237**: 499–507.

Nishiizumi K, Imamura M, Caffee MW, Southon JR, Finkel RC, McAninch J. 2007. Absolute calibration of 10Be AMS standards. *Nuclear Instruments and Methods in Physics Research* **Section B**: 403–413.

Norton KP, Abbühl LM, Schlunegger F. 2010. Glacial conditioning as an erosional driving force in the Central Alps. *Geology* **38**: 655–658.

Oskin M, Burbank DW. 2005. Alpine landscape evolution dominated by cirque retreat. *Geology* **33**: 933–936.

Osmaston H. 1994. The geology, geomorphology and Quaternary history of Zangskar. In *Himalayan Buddhist Villages*. Crook J, Osmaston H (eds). University of Bristol Press: Bristol, UK; 1–36.

Osmaston H. 2005. Estimates of glacier equilibrium line altitudes by the area × altitude, the area × altitude balance ratio and the area × altitude balance index methods and their validation. *Quaternary International* **138–139**: 22–31.

Owen LA. 2009. Latest Pleistocene and Holocene glacier fluctuations in the Himalaya and Tibet. *Quaternary Science Reviews* **28**: 2150–2164.

Owen LA, Finkel RC, Barnard PL, Ma H, Asahi K, Caffee MW, Derbyshire E. 2005. Climatic and topographic controls on the style and timing of Late Quaternary glaciation throughout Tibet and the Himalaya defined by ^{10}Be cosmogenic radionuclide surface exposure dating. *Quaternary Science Reviews* **24**: 1391–1411.

Owen LA, Caffee M, Bovard K, Finkel RC, Sharma M. 2006. Terrestrial cosmogenic surface exposure dating of the oldest glacial successions in the Himalayan orogen. *Geological Society of America Bulletin* **118**: 383–392.

Owen LA, Caffee MW, Finkel RC, Seong BS. 2008. Quaternary glaciation of the Himalayan–Tibetan orogeny. *Journal of Quaternary Science* **23**: 513–532.

Owen LA, Dortch JM. 2014. Nature and timing of Quaternary glaciation in the Himalayan-Tibetan orogen. *Quaternary Science Reviews* **88**: 13–54.

Parker G, Perg LA. 2005. Probabilistic formulation of conservation of cosmogenic nuclides: effect of surface elevation fluctuations on approach to steady state. *Earth Surface Processes and Landforms* **30**: 1127–1144.

Pazzaglia FJ, Brandon MT. 2001. A fluvial record of long term steady-state uplift and erosion across the Cascadia forearc high, western Washington State. *American Journal of Science* **301**: 385–431.

Pedersen VK, Egholm DL. 2013. Glaciations in response to climate variations preconditioned by evolving topography. *Nature* **493**: 206–210.

Portenga EW, Bierman PR. 2011. Understanding Earth's eroding surface with ^{10}Be. *GSA Today* **21**: 4–10.

Reinhardt LJ, Hoey TB, Barrows TT, Dempster TJ, Bishop P, Fifield LK. 2007. Interpreting erosion rates from cosmogenic radionuclide concentratins measured in rapidly eroding terrain. *Earth Surface Processes and Landforms* **32**: 390–406.

Riebe CS, Kirchner JW, Granger DE, Finkel RC. 2001. Strong tectonic and weak climatic control of long-term chemical weathering rates. *Geology* **29**: 511–514.

Searle MP. 1991. *Geology and Tectonics of the Karakoram Mountains*. John Wiley and Sons: Chichester, UK.

Shi Y, Yu G, Liu X, Li B, Yao T. 2001. Reconstruction of the 30–40 ka BP enhanced Indian monsoon climate based on geological records from the Tibetan Plateau. *Paleogeography, Paleoclimatology, Paleoecology* **169**: 69–83.

Shroder JF Jr, Bishop MP. 2000. Unroofing of the Nanga Parbat Himalaya. *Geological Society Special Publications* **170**: 163–179.

Slaymaker O. 2011. Criteria to distinguish between periglacial, proglacial and paraglacial environments. *Quaestiones Geographicae* **30**: 85–94. DOI: 10.2478/v10117-011-0008-y

Small EE, Anderson RS, Repka JL, Finkel RC. 1997. Erosion rates of alpine bedrock summit surfaces deduced from in-situ Be-10 and Al-26. *Earth and Planetary Science Letters* **150**: 413–425.

Sorkhabi RB, Foland KA, Jain AK, Manickavasagam RM. 1999. Tectonic and cooling history of the Garhwal Higher Himalaya, Bhagirathi Valley: constraints from thermochronological data. *Gondwana Research Group Memoir* **6**: 217–235.

Spotila JA. 2012. Influence of drainage divide structure on the distribution of mountain peaks. *Geology* **40**: 855–858.

Spotila JA. 2013. Glacially influenced tectonic geomorphology: the impact of the glacial buzzsaw on topography and orogenic systems. In *Tectonic Geomorphology. Treatise in Geomorphology 5*, Owen LA (ed). Academic Press: San Diego; 300–317.

Steck A. 2003. Geology of the NW Indian Himalaya. *Eclogae Geologicae Helvetiae* **96**: 13–196.

Stock GM, Ehlers TA, Farley KA. 2006. Where does sediment come from? Quantifying catchment erosion with detrital apatite (U-Th)/He thermochronometry. *Geology* **34**: 725–728.

Strobl M, Hetzel R, Niedermann S, Ding L, Zhang L. 2012. Landscape evolution of a bedrock peneplain on the southwestern Tibetan Plateau revealed by in situ-produced cosmogenic ^{10}Be and ^{21}Ne. *Geomorphology* **153-154**: 192–204.

Thiede RC, Arrowsmith JR, Bookhagen B, McWilliams MO, Sobel ER, Strecker MR. 2005. From tectonically to erosionally controlled development of the Himalayan orogen. *Geology* **33**: 689–692.

Thomson SN, Brandon MT, Tomkin JH, Reiners PW, Vásquez C, Wilson NJ. 2010. Glaciation as a destructive and constructive control on mountain building. *Nature* **467**: 313–317.

Tripathy-Lang A, Hodges KV, Monteleone BD, van Soest MC. 2013. Laser (U-Th)/He thermochronology of detrital zircons as a tool for studying surface processes in modern catchments. *Journal of Geophysical Research, Earth Surface* **118**: 1–9. DOI: 10.1002/jgrf.20091

Vannay J-C, Grasemann B, Rahn M, Frank W, Carter A, Baudraz V, Cosca M. 2004. Miocene to Holocene exhumation of metamorphic crustal wedges in the NW Himalaya: evidence for tectonic extrusion coupled to fluvial erosion. *Tectonics* **23**: TC1014. DOI: 10.1029/2002TC001429

weatherbase.com, 2013. http://www.weatherbase.com/weather/weather.php3?s=44534&cityname=Leh-India [Accessed 16 May 2013].

Wellman HW, Wilson AT. 1965. Salt weathering, a neglected geological erosive agent in coastal and arid environments. *Nature* **205**: 1097–1098. http://www.nature.com/nature/journal/v205/n4976/pdf/2051097a0.pdf [Accessed 15 November 2013].

Ward DJ, Anderson RS, Haeussler PJ. 2012. Scaling the Teflon Peaks: rock type and the generation of extreme relief in the glaciated western Alaska Range. *Journal of Geophysical Research* **117**: F01031. DOI: 10.1029/2011JF002068

Whipple KX. 2004. Bedrock rivers and the geomorphology of active orogens. *Annual Reviews of Earth and Planetary Sciences* **32**: 151–185.

Willet SD, Brandon MT. 2002. On steady states in mountain belts. *Geology* **30**: 175–178.

Wobus C, Heimsath A, Whipple K, Hodges K. 2005. Active out-of-sequence thrust faulting in the central Nepalese Himalaya. *Nature* **434**: 1008–1011.

Zeitler P. 2014. The fate of orogens: How do exhumation processes scale across time? *Geological Society of America Abstracts with Programs* **46/2**: 94.

